identically well-defined value of the internuclear distance during the transition and, consequently, any possible direct energy exchange between electronic and nuclear motions was neglected. For example, in such a model, the electron energy from the path shown by an orange line in Fig. 1E (resonant photoionization through the $2p\sigma_u$ channel) would be equal to the energy difference between the $Q_2$ and the $2p\sigma_u$ curve at the marked internuclear distance. Similar reasoning predicts the electron energy along the path shown by the green line (resonant photoionization through the $1s\sigma_g$ channel). Our calculations show that, in this case, although such simplified models have heuristic and pedagogical value, they lead to false conclusions. The model predicts that the maximum possible value of the KER in the $1s\sigma_g$ channel is 8.1 eV (corresponding to an autoionization decay at infinite internuclear distance), which is the minimum possible value of the KER in the $2p\sigma_u$ channel (corresponding to autoionization decay at the equilibrium internuclear distance). Therefore, no interference between g and u states can occur within this model because the electron energies and the KER regions for transitions to $1s\sigma_g$ and $2p\sigma_u$ would have no overlap, and hence the electron ejection would always be symmetric. Our fully quantum mechanical treatment showed that transitions to the $1s\sigma_g$ state can occur beyond 8.1 eV and that transitions to the $2p\sigma_u$ state are possible even at zero KER. Thus, the angular distribution can exhibit an asymmetry over the whole region of KER. Strictly speaking, a symmetric dissociation in the presence of resonances is the exception rather than the rule. It becomes quantitatively substantial in the region where both channels are comparably active, between 8 and 10 eV; however, it is also visible in regions where one of the channels dominates (Fig. 3A, b to f).

Notably, the observed asymmetry has no relation to the direction in which the charged fragment is emitted: The larger lobes are sometimes found on the ion side (Fig. 3A, c, d, and e) and sometimes on the neutral side (Fig. 3A, b and f). Both theory and experiment show that the asymmetry oscillates with the KER and that the amplitude of these oscillations is more important in the region where the $1s\sigma_g$ and $2p\sigma_u$ channels overlap. Between consecutive oscillations, there are KER values for which the distribution is practically symmetric. Thus, the asymmetry cannot be explained by a preferred attractive interaction between the proton and the escaping electron (the latter is too fast to be efficiently perturbed by the slow proton, except possibly in the region of the maximum allowed KER).

Asymmetric photoelectron angular distributions should arise in any symmetric molecule that decays through two (or more) dissociative ionization channels associated with different symmetries of the residual molecular ion. When the final electron energy is the same in both channels, the corresponding ionization pathways are indistinguishable. This equivalence leads to interferences that depend on the time delay between the two ionization processes. The time delay implies that the decay in either pathway occurs at different positions of the nuclei. This unique relationship between time delay and nuclear positions makes the problem of molecular autoionization much richer than the atomic case, and the asymmetry of the photoelectron angular distribution its most noteworthy (and so far unexpected) effect. Symmetry breaking should be considered a general molecular manifestation of autoionization when several decay channels are effectively accessible.

### References and Notes

1. I. N. Levine, *Molecular Spectroscopy* (Wiley, New York, 1975).
2. D. Rolles *et al.*, *Nature* **437**, 711 (2005).
3. G. Herzberg, *Molecular Spectra and Molecular Structure*, vol. III of *Electronic Spectra and Electronic Structure of Polyatomic Molecules* (Prentice-Hall, New York, 1979).
4. M. F. Kling *et al.*, *Science* **312**, 246 (2006).
5. R. Dörner *et al.*, *Phys. Rep.* **330**, 95 (2000).
6. J. Ullrich *et al.*, *Rep. Prog. Phys.* **66**, 1463 (2003).
7. U. Fano, *Phys. Rev.* **124**, 1866 (1961).
8. S. Strathdee, R. Browning, *J. Phys. B* **12**, 1789 (1979).
9. C. J. Latimer, J. Geddes, M. A. McDonald, N. Kouchi, K. F. Dunn, *J. Phys. B* **29**, 6113 (1996).
10. K. Ito, R. I. Hall, M. Ukai, *J. Chem. Phys.* **104**, 8449 (1996).
11. M. Lebech *et al.*, *Phys. Rev. Lett.* **96**, 073001 (2006).
12. C. Bottcher, K. Docken, *J. Phys. B* **7**, L5 (1974).
13. I. Sánchez, F. Martín, *Phys. Rev. A.* **60**, 2200 (1999).
14. A. Lafosse *et al.*, *J. Phys. B* **36**, 4683 (2003).
15. A. V. Golovin *et al.*, *Phys. Rev. Lett.* **79**, 4554 (1997).
16. D. Dill, *J. Chem. Phys.* **65**, 1130 (1976).
17. I. Sánchez, F. Martín, *Phys. Rev. Lett.* **82**, 3775 (1999).
18. F. Martín, *J. Phys. B* **32**, R197 (1999).
19. H. Bachau, E. Cormier, P. Decleva, J. E. Hansen, F. Martín, *Rep. Prog. Phys.* **64**, 1815 (2001).
20. G. Laurent *et al.*, *Phys. Rev. Lett.* **96**, 173201 (2006).
21. W. Vanroose, F. Martín, T. N. Rescigno, C. W. McCurdy, *Science* **310**, 1787 (2005).
22. O. Jagutzki *et al.*, *Nucl. Instrum. Methods* **A477**, 244 (2002).
23. T. Jahnke *et al.*, *J. Electron Spectrosc. Relat. Phenom.* **141**, 229 (2004).
24. This work was supported in part by Dirección General de Investigación project no. BFM2003-00194; the European Cooperation in the field of Scientific and Technical Research (COST) action D26/0002/02; Bundesministerium für Bildung und Forschung; Deutsche Forschungsgemeinschaft; Deutscher Akademischer Austauschdienst; the Division of Chemical Sciences, Geosciences and Biosciences Division, Office of Basic Energy Sciences, Office of Science, U.S. Department of Energy; and the Director, Office of Science, Office of Basic Energy Sciences and Division of Materials Sciences under U.S. Department of Energy contract no. DE-AC03-76SF00098. We thank Roentdek GmbH (www.roentdek.com) for support with the delay-line detectors; the Centro de Computación Científica of the Universidad Autónoma de Madrid for its generous allocation of computer time; D. Dowek for discussions related to the effects observed in her group; H. J. Lüdde for discussions; and the staff at Advanced Light Source, in particular B. S. Mun, for support.

23 October 2006; accepted 8 December 2006
10.1126/science.1136598

# Ultrafast Bond Softening in Bismuth: Mapping a Solid's Interatomic Potential with X-rays

D. M. Fritz,[1,2*] D. A. Reis,[1,2] B. Adams,[3] R. A. Akre,[4] J. Arthur,[5] C. Blome,[6] P. H. Bucksbaum,[2,4,7] A. L. Cavalieri,[8] S. Engemann,[5] S. Fahy,[9] R. W. Falcone,[10] P. H. Fuoss,[11] K. J. Gaffney,[5] M. J. George,[5] J. Hajdu,[12] M. P. Hertlein,[13] P. B. Hillyard,[14] M. Horn-von Hoegen,[15] M. Kammler,[16] J. Kaspar,[14] R. Kienberger,[8] P. Krejcik,[4] S. H. Lee,[17] A. M. Lindenberg,[5] B. McFarland,[7] D. Meyer,[15] T. Montagne,[4] É. D. Murray,[9] A. J. Nelson,[18] M. Nicoul,[15] R. Pahl,[19] J. Rudati,[3] H. Schlarb,[6] D. P. Siddons,[20] K. Sokolowski-Tinten,[15] Th. Tschentscher,[6] D. von der Linde,[15] J. B. Hastings[5]

Intense femtosecond laser excitation can produce transient states of matter that would otherwise be inaccessible to laboratory investigation. At high excitation densities, the interatomic forces that bind solids and determine many of their properties can be substantially altered. Here, we present the detailed mapping of the carrier density–dependent interatomic potential of bismuth approaching a solid-solid phase transition. Our experiments combine stroboscopic techniques that use a high-brightness linear electron accelerator–based x-ray source with pulse-by-pulse timing reconstruction for femtosecond resolution, allowing quantitative characterization of the interatomic potential energy surface of the highly excited solid.

The availability of bright sources of ultrafast hard x-rays, such as future free-electron lasers, opens up the possibility to follow atomic motion stroboscopically with the picometer spatial and femtosecond temporal resolution required to capture the fastest atomic vibrations and the making and breaking of chemical bonds (*1*). However, the inability to precisely time the x-ray probe can lead to significant reduction in temporal resolution. Recently, the use of single-shot determination of the x-ray arrival time as a means of random sampling has been demonstrated to circumvent this problem (*2*). Using this technique, we con-

ducted femtosecond laser-pump x-ray–probe experiments that elucidate the role that carrier-induced bond-softening and anharmonicity play in the high-amplitude phonon dynamics of photoexcited bismuth.

The valence electrons and ionic cores (nucleus and core electrons) that constitute a crystalline solid, in general, can be considered as distinct components that couple through the electron-lattice interaction. In bismuth, as well as antimony and tellurium, the electron-lattice interaction is strong and the lattice configuration is sensitive to the population distribution of electrons within the conduction bands. In these materials, femtosecond photoexcitation of charge carriers drives the symmetric zone center $A_{1g}$ coherent optical phonon mode (*3*–*5*). The vibrational excitation is generally believed to be displacive: The population redistribution of valence electrons alters the potential energy surface of the lattice and gives rise to a restoring force that drives coherent atomic motion. The dynamics of this mode are determined by the curvature and minima location of the altered potential energy surface (quasi-equilibrium coordinate). Knowledge of electronically excited energy surfaces is essential for predictive models of nonequilibrium behavior in this and a wider class of important processes in nature (from photocatalysis to nonequilibrium charge transport in nanojunctions).

Experimentally, the $A_{1g}$ vibrational mode has been monitored indirectly by measuring time-dependent optical reflectivity (*3*, *6*–*10*) and directly by time-resolved x-ray diffraction measurements (*11*). However, with the latter technique, low x-ray flux prevented carrier-dependent studies of the interatomic potential. Recent observations in bismuth and tellurium reveal that the vibrational frequency is not constant: It red-shifts from the equilibrium value under high-intensity excitation, indicating a softened phonon mode (*7*, *9*–*12*). After the initial softening, the oscillation frequency blue-shifts back toward the equilibrium value as the oscillation amplitude and carrier density decay (*9*, *10*). The mechanism responsible for this time-dependent vibrational frequency shift, or chirp, has been controversial. Hase *et al*. concluded that the chirp was due to an amplitude-dependent frequency caused by anharmonicity of the interatomic potential (*9*). Fahy and Reis suggested an alternate explanation based on electronic softening of the potential and the subsequent dynamics of the photoexcited carriers (*13*). Optical coherent control experiments in which the phonon amplitude was varied at fixed electronic excitation demonstrated that the observed phonon frequency is dominated by electronic effects and that anharmonicity in the interatomic potential plays a negligible role, a finding that was supported by ab initio constrained density functional theory (DFT) calculations (*10*). However, because optical reflectivity does not measure atomic positions, the location of the potential energy minimum and the amplitude of the phonon-driven atomic displacement could not be determined.

We used femtosecond x-ray diffraction to elucidate the dynamics of the high-amplitude phonons by direct measurement of the atomic positions within the unit cell. The knowledge of the time evolution of the atomic positions enables the determination of the quasi-equilibrium coordinate and curvature of the interatomic potential and the comparison of these parameters to previous DFT calculations. The potential well shifts and softens with increasing carrier density, corresponding to a highly excited solid in which a substantial fraction of the total valence electrons are promoted to the conduction bands.

The room temperature structure of bismuth is rhombohedral A7 with two atoms per unit cell. This structure is a Peierls distortion of a simple cubic structure, with alternating atoms spaced nonequidistantly along the body diagonal or trigonal axis. Thus, there exists a double-well interatomic potential with normalized equilibrium coordinate at $x = 0.5 \pm \delta$ (in units of the hexagonal unit cell length, $c = 1.18$ nm). The $A_{1g}$ mode consists of an oscillation of the two basis atoms along the trigonal direction, and thus $x$ is also the phonon coordinate. $\delta$ is a measure of the Peierls distortion, that is, the deviation of each potential energy minimum from the symmetric $x = 0.5$ point. The quasi-equilibrium coordinate and shape of the well constraining the atoms along the trigonal direction are sensitive to excitation of carriers from the valence band to the conduction band (*10*).

A 50-nm-thick bismuth film grown by molecular beam epitaxy with a (111) surface orientation (*14*) was excited at room temperature by near-infrared pulses [(70 fs full width at half maximum (FWHM)] propagating from a Ti:sapphire laser system in a direction colinear with the x-rays. The x-ray pulses ($10^6$ photons at 9 keV, 0.24 mm$^2$ area, 100 fs duration) were generated from the Sub-Picosecond Pulse Source (SPPS) at the Stanford Linear Accelerator Center (SLAC). The (111) x-ray Bragg reflection was observed for absorbed excitation fluences between 0.3 and 3.0 mJ/cm$^2$ per pulse at a 10 Hz repetition rate (*15*). We note that at 1.5 mJ/cm$^2$, enough energy is deposited to eventually raise the temperature of the entire film to the melting point, although at least 4.1 mJ/cm$^2$ is required to provide the additional latent heat for thermal melting. It is in this high fluence regime that ultrafast excitation of carriers generates large-amplitude coherent phonons with a significantly lowered frequency.

During the first few picoseconds after excitation, it appears that the absorbed energy is stored almost entirely in the electronic degrees of freedom and the mechanical vibration associated with the $A_{1g}$ mode. In this time, the volume of the unit cell remains fixed and the

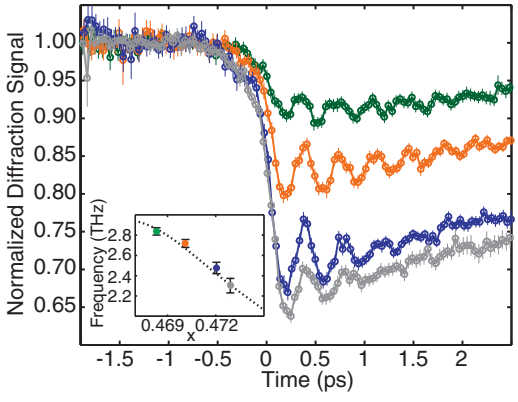


**Fig. 1.** Bismuth (111) x-ray diffraction efficiency as a function of time delay between the optical excitation pulse and x-ray probe for excitation fluences of 0.7 (green), 1.2 (red), 1.7 (blue), and 2.3 mJ/cm$^2$ (gray). The zero-delay point was set at the half maximum of the initial transient drop. The inset displays the optical phonon frequency as a function of the normalized atomic equilibrium position along the body diagonal of the unit cell $x$ as measured by x-ray diffraction. The dotted curve represents the theoretical prediction obtained from DFT calculations of the excited-state potential-energy surface (*10*).

[1]Frontiers in Optical Coherent and Ultrafast Science (FOCUS) Center, Departments of Physics and Applied Physics Program, University of Michigan, Ann Arbor, MI 48109, USA. [2]Photon Ultrafast Laser Science and Engineering (PULSE) Center, Stanford Linear Accelerator Center, Menlo Park, CA 94025, USA. [3]Advanced Photon Source, Argonne National Laboratory, Argonne, IL 60439, USA. [4]Stanford Linear Accelerator Center (SLAC), Menlo Park, CA 94025, USA. [5]Stanford Synchrotron Radiation Laboratory/SLAC, Menlo Park, CA 94025, USA. [6]Deutsches Elektronen-Synchrotron DESY, Notkestrasse 85, 22607 Hamburg, Germany. [7]Departments of Physics and Applied Physics, Stanford University, Stanford, CA 94305, USA. [8]Max-Planck-Institute of Quantum Optics, Hans-Kopfermann-Strasse 1, D-85748 Garching, Germany. [9]Department of Physics and Tyndall National Institute, University College, Cork, Ireland. [10]Department of Physics, University of California, Berkeley, CA 94720, USA. [11]Materials Science Division, Argonne National Laboratory, Argonne, IL 60439, USA. [12]Department of Cell and Molecular Biology, Biomedical Centre, Uppsala University, SE-75124 Uppsala, Sweden. [13]Lawrence Berkeley National Laboratory, Berkeley, CA 94720, USA. [14]Department of Chemistry, Stanford University, Stanford, CA 94305, USA. [15]Institut für Experimentelle Physik, Universität Duisburg-Essen, 47057 Duisburg, Germany. [16]Institut für Halbleitertechnologie, Universität Hannover, Hannover, Germany. [17]Korea Research Institute of Standards and Science, Daejeon 305-600, Republic of Korea. [18]Lawrence Livermore National Laboratory, Livermore, CA 94550, USA. [19]Consortium for Advanced Radiation Sources, University of Chicago, Chicago, IL 60637, USA. [20]National Synchrotron Light Source, Brookhaven National Laboratory, Upton, NY 11973, USA.

*To whom correspondence should be addressed. E-mail: dmfritz@slac.stanford.edu

lattice remains at room temperature. On the time scale of ~20 picoseconds, considerable uniaxial strain is observed as a shift in the Bragg angle. Thus, the observed changes in the diffraction efficiency at these early times (Fig. 1) are due to structural changes within the unit cell of the crystal. The structure factor for the (hkl) Bragg reflection is a function of the phonon coordinate

$$F = 2f_{Bi} \cos[\pi (h + k + l) x] \quad (1)$$

where $f_{Bi}$ is the atomic scattering factor for bismuth. In the limit of a thin film and constant temperature, the normalized diffraction signal for the (111) reflection is a direct measure of the atomic displacement along the trigonal direction

$$I(t) / I(0) = \cos^2[3\pi x(t)] / \cos^2[3\pi x(0)] \quad (2)$$

A large transient decrease in diffraction efficiency occurs upon the arrival of the excitation pulse ($t = 0$) and is followed by damped oscillations superimposed upon a recovery. In the high-symmetry, non-Peierls distorted state, $x = 0.5$ and the (111) reflection is forbidden by symmetry. Thus, the transient decrease is attributed to a sudden shift in the minima location of the potential energy surface (toward $x = 0.5$) in the excited electronic state, leading to atomic oscillations about the shifted equilibrium. Measurements of the (222) reflection, which increases in intensity for the higher-symmetry arrangement, confirm this attribution. A similar behavior was observed by Sokolowski-Titen *et al*. (*11*). The quasi-equilibrium coordinate is then measured directly from the magnitude of the transient decrease of the relative diffraction efficiency seen in the (111) data (i.e., from the value about which the oscillations occur). The subsequent increase is ascribed to carrier relaxation through diffusion and recombination, which eventually restores the potential energy surface to its equilibrium shape at excitation levels below the damage threshold.

The oscillatory part of the diffraction signal, corresponding to the coherent optical phonon mode, was fit to a decaying sinusoid with fixed frequency and varying initial phase. Because the phonon frequency is chirped, the frequency obtained from the fit represents the average phonon frequency over the fitting interval (~0.5 to 1.5 ps). The measured value, ranging from 2.84 to 2.31 THz, is red-shifted relative to that observed in continuous wave Raman scattering experiments (2.93 THz) (*8*). Similar softening has been measured in optical experiments (*7*, *9*, *10*).

The inset of Fig. 1 displays the dependence of phonon frequency on the quasi-equilibrium coordinate (measured over the same time interval as the phonon frequency). Our results also represent average values over the sample depth for both frequency and quasi-equilibrium coordinate, because the x-ray penetration depth is much larger than the film thickness. In the absence of photoexcitation, the accepted values of the frequency and equilibrium location at room temperature are 2.93 THz and $x = 0.46719$ (*10*, *16*–*18*). At a measured quasi-equilibrium coordinate of $x = 0.4729 \pm 0.0001$, the well is shifted by 6.7 picometers and the interatomic forces are softened by 35% (~20% decrease in the phonon frequency). The results are compared with the constrained DFT calculation of Murray *et al*. (*10*) (dotted line). These first-principles calculations assumed production of a single electron-hole pair per absorbed photon and rapid thermalization of the electrons and holes by intraband scattering, followed by electron-hole recombination on a longer time scale. Therefore, the electron and hole distributions are approximated as independent Fermi-Dirac distributions with separate chemical potentials such that the average energy of each pair is equal to the photon energy. Despite these approximations, the excellent agreement with experimental results here demonstrates the ability of DFT to quantitatively predict the essential excited-state features (quasi-equilibrium coordinate and frequency) of this system.

Under the same assumption of a single electron-hole pair produced per absorbed photon, we separately compare the measured quasi-equilibrium coordinate as a function of carrier density to the DFT predictions (Fig. 2). The calculated double-well potential with the quasi-equilibrium coordinate is indicated by the dotted line (for illustrative purposes we arbitrarily chose the $x < 0.5$ well). The curving of the dotted line toward $x = 0.5$ shows that increasing carrier density reduces the Peierls distortion. The shift in equilibrium coordinate was measured for carrier densities spanning 0.18% to 1.8% of the total valence electrons, averaged over the 50-nm film. A transient displacement of 11 picometers was observed for the highest carrier density and corresponds to 2.0% of the equilibrium interatomic separation along the trigonal axis. This value is not the same as the change in nearest-neighbor distance, which is smaller by a factor of about two. Higher excitation levels led to irreversible damage to the material, which was evident as an overall decrease in the diffraction efficiency for the unexcited crystal.

The calculations suggest that upon excitation of ~2.5% of the valence electrons, bismuth undergoes a structural phase transition to a higher symmetry state, whereas at approximately 2% excitation the barrier between the wells is lowered sufficiently for the atoms to move in both wells (*19*). It is unclear, for an initial room temperature lattice, whether this level of excitation density can be achieved without subsequent thermal melting of the material (or what role formation of domains plays in the melting transition). At these excitation levels there is no

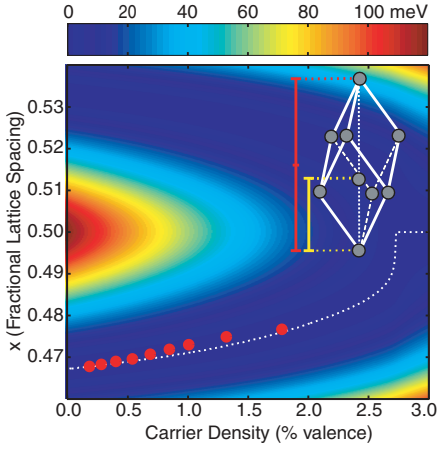


**Fig. 2.** Interatomic quasi-equilibrium position as a function of the percentage of valence electrons promoted into the conduction band. The red circles represent experimental results; the dotted line depicts the potential minimum obtained from the DFT potential landscape. The adjusted potential energy surface obtained from DFT is overlayed in false color representation (*10*). The bismuth unit cell is displayed in the upper right quadrant. The red bar represents the body diagonal length *c*, and the yellow bar represents the basis atom coordinate *xc*.

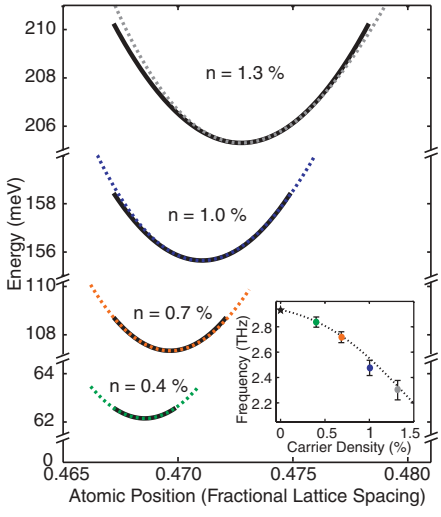


**Fig. 3.** Interatomic potential curvature as a function of carrier density *n*. Solid lines represent the region of the interatomic potential sampled by the atoms under complete displacive excitation. The curvature was derived from the measured phonon frequency, assuming pure harmonic motion. Dotted lines are cross sections of the DFT interatomic potential surface displayed in Fig. 2 for fixed carrier densities. The vertical scale is adjusted for clarity, and the potential energy is displayed relative to the minimum of the unexcited structure. The inset displays the phonon frequency as a function of carrier density. The dotted line shows *A1g* frequencies from DFT frozen phonon calculations. The starred point is the equilibrium Raman value of the A1g frequency.

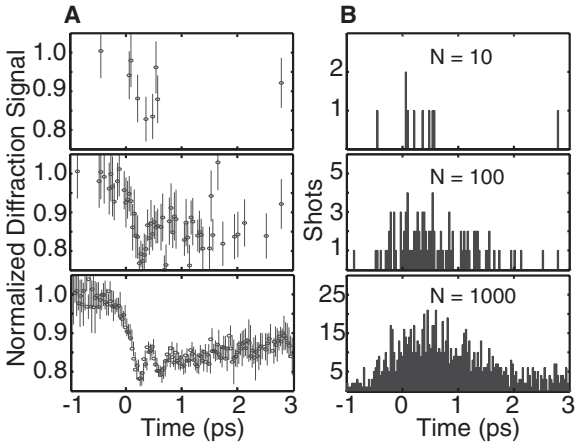


**Fig. 4.** (**A**) X-ray data arranged sequentially by the arrival time determined by electro-optic sampling for $N$ = 10, 100, and 1000 shots. (**B**) Corresponding histograms of the measured electron bunch arrival times. A movie of the data acquisition is included as supporting online material.

evidence, either experimentally or in the DFT results, of a nonthermal melting transition such as that found in tetrahedrally bonded semiconductors (*20*–*24*).

In addition to the quasi-equilibrium coordinate, we extract the carrier density–dependent curvature of the potential well from the measured frequency of the $A1g$ mode, assuming a harmonic potential (solid black curves in Fig. 3). The extent of the curves represents the maximum range of motion of the ions that occurs in the limit of a purely displacive excitation. A comparison of these results with the potential calculated by DFT (dotted lines, corresponding to fixed-density cross sections of the surface shown in Fig. 2) shows that for carrier densities as high as 1%, the atoms are well described as moving in a purely harmonic potential. At the highest carrier density in which we could extract a phonon frequency from the data, the calculations predict only a slight deviation from a harmonic potential. This result is reinforced by the excellent agreement between the measured and calculated frequency (which includes the anharmonic terms) as a function of carrier density (Fig. 3, inset). Thus, although anharmonicity must be present at some level, electronic softening by far dominates the determination of the phonon frequency at the high excitation densities in this and former experiments.

Two important technical advances enabled these experiments: the generation of high x-ray photon flux in a temporally short pulse from a linear accelerator source and the ability to measure the relative x-ray and laser pulse arrival times. Standard stroboscopic measurements in the subpicosecond time regime derive the excitation pulse and probe pulse from the same ultrafast source with the pump-probe relative delay determined by the optical path length difference. This setup ensures synchronization between pump and probe and realizes the temporal limit set by the probe pulse duration. In experiments in which the pump and probe are derived from separate sources, such as the study reported here, synchronization is not inherent and must be actively attained. To achieve temporal resolution of the order of x-ray pulse duration, it is necessary to either synchronize the two sources to a fraction of the probe pulse duration or to measure the relative arrival time on a shot-by-shot basis. As a result of sources of jitter in the linear electron accelerator that cannot be mitigated, particularly electron bunch energy fluctuations, synchronization to the level of the x-ray pulse duration is not achievable and a relative time-of-arrival measurement is essential for experiments that require multishot data acquisition.

Temporal resolution of ~100 fs, required to observe coherent phonon motion in bismuth, was achieved by measuring the relative arrival time of the electron bunches using electro-optic sampling (EOS) (*2*). Laser pulses, split from the same source used to photoexcite the bismuth film, were transported by optical fiber to the electron beam (*25*). The measured electro-optic signal from the electron bunch was as short as 170 fs FWHM, and the centroid of this feature was determined to sub-20 fs precision and used as a time stamp for the relative time of arrival. The temporal jitter between the pump and the probe provided random sampling of time points. X-ray data obtained from diffraction measurements were sorted into 40-fs time bins according to the time of arrival measured through EOS (Fig. 4). Data within a time bin were averaged together to increase the signal-to-noise ratio. The results of these experiments demonstrate the type of data collection techniques and timing diagnostic that will be instrumental to maximize the scientific capabilities of the next generation of x-ray light sources.

### References and Notes


1. R. F. Service, *Science* **298**, 1356 (2002).
2. A. L. Cavalieri *et al.*, *Phys. Rev. Lett.* **94**, 114801 (2005).
3. T. K. Cheng *et al.*, *Appl. Phys. Lett.* **59**, 1923 (1991).
4. H. J. Zeiger *et al.*, *Phys. Rev. B* **45**, 768 (1992).
5. T. Stevens, J. Kuhl, R. Merlin, *Phys. Rev. B* **65**, 144304 (2002).
6. T. K. Cheng *et al.*, *Appl. Phys. Lett.* **57**, 1004 (1990).
7. M. F. DeCamp, D. A. Reis, P. H. Bucksbaum, R. Merlin, *Phys. Rev. B* **64**, 092301 (2001).
8. M. Hase, K. Mizoguchi, H. Harima, S. Nakashima, K. Sakai, *Phys. Rev. B* **58**, 5448 (1998).
9. M. Hase, M. Kitajima, S. Nakashima, K. Mizoguchi, *Phys. Rev. Lett.* **88**, 67401 (2002).
10. E. D. Murray, D. M. Fritz, J. K. Wahlstrand, S. Fahy, D. A. Reis, *Phys. Rev. B* **72**, 060301(R) (2005).
11. K. Sokolowski-Tinten *et al.*, *Nature* **422**, 287 (2003).
12. S. Hunsche, K. Wienecke, T. Dekorsy, H. Kurz, *Phys. Rev. Lett.* **75**, 1815 (1995).
13. S. Fahy, D. A. Reis, *Phys. Rev. Lett.* **93**, 109701 (2004).
14. M. Kammler, M. Horn-von Hoegen, *Surf. Sci.* **576**, 56 (2005).
15. The absorbed laser energy was measured by subtracting the reflected laser energy from the incident energy. The absorbed fluence was then computed with knowledge of the laser intensity profile. This measurement takes into account the optical properties of bismuth for the particular incidence angle and laser polarization used. Only the incident fluence was stated in many of the cited references, and therefore the optical properties of bismuth must be taken into account before directly comparing the results.
16. P. Fischer, I. Sosnowska, M. Szymanski, *J. Phys. C Solid State Phys.* **11**, 1043 (1978).
17. X. Gonze, J.-P. Michenaud, J.-P. Vigneron, *Phys. Rev. B* **41**, 11827 (1990).
18. An experimental ambiguity regarding the room temperature equilibrium position exists: A measurement of 0.4668 was cited in (*14*) and 0.46814 was cited in (*15*). The chosen value of 0.46719, the equilibrium value determined by DFT, was used to best compare experimental results to DFT calculations.
19. This phase transition is distinct from the Bi I-II transition that occurs at 25.3 kbar of hydrostatic pressure (*26*).
20. R. Biswas, V. Ambegaokar, *Phys. Rev. B* **26**, 1980 (1982).
21. C. V. Shank, R. Yen, C. Hirlimann, *Phys. Rev. Lett.* **50**, 454 (1983).
22. P. Stampfli, K. H. Bennemann, *Phys. Rev. B* **49**, 7299 (1994).
23. A. M. Lindenberg *et al.*, *Science* **308**, 392 (2005).
24. V. Recoules, J. Cl'erouin, G. Z'erah, P. M. Anglade, S. Mazevet, *Phys. Rev. Lett.* **96**, 055503 (2006).
25. S. H. Lee, A. L. Cavalieri, D. M. Fritz, M. Myaing, D. A. Reis, *Opt. Lett.* **29**, 2602 (2004).
26. P. W. Bridgman, *Proc. Am. Acad. Arts Sci.* **74**, 438 (1942).


27. Portions of this research were supported by the U.S. Department of Energy, Office of Basic Energy Science through direct support for the SPPS and individual investigators and through the Stanford Synchrotron Radiation Laboratory, a national user facility operated by Stanford University, and the University of California Lawrence Livermore National Laboratory. Additional support for the construction of SPPS was provided by Uppsala University through a grant from the Swedish Research Council. E.D.M. is supported by the Irish Research Council for Science, Engineering, and Technology, S.F. by Science Foundation Ireland, and J.K. by the Keck Foundation. M.N., K.S.T. and D.V.D.L. gratefully acknowledge support by the Deutsche Forschungsgemeinschaft and the European Union [Research Training Network (RTN) Free-electron Laser in Hamburg (FLASH)]. R.K. acknowledges a fellowship of the Austrian Academy of Sciences. D.M.F. and D.A.R. were supported by the NSF FOCUS frontier center and Stanford PULSE center.


### Supporting Online Material

www.sciencemag.org/cgi/content/full/315/5812/633/DC1
Movie S1

12 September 2006; accepted 19 December 2006
10.1126/science.1135009

# ERRATUM

*Post date 16 February 2007*

**Reports**: "Ultrafast bond softening in bismuth: Mapping a solid's interatomic potential with x-rays" by D. M. Fritz *et al*. (2 Feb. 2007, p. 633). In the acknowledgments note (*27*), one of the funding groups was misidentified. FLASH stands for "Understanding Fast Light-Actuated Structural Changes."

# Ultrafast Bond Softening in Bismuth: Mapping a Solid's Interatomic Potential with X-rays

D. M. Fritz, D. A. Reis, B. Adams, R. A. Akre, J. Arthur, C. Blome, P. H. Bucksbaum, A. L. Cavalieri, S. Engemann, S. Fahy, R. W. Falcone, P. H. Fuoss, K. J. Gaffney, M. J. George, J. Hajdu, M. P. Hertlein, P. B. Hillyard, M. Horn-von Hoegen, M. Kammler, J. Kaspar, R. Kienberger, P. Krejcik, S. H. Lee, A. M. Lindenberg, B. McFarland, D. Meyer, T. Montagne, É. D. Murray, A. J. Nelson, M. Nicoul, R. Pahl, J. Rudati, H. Schlarb, D. P. Siddons, K. Sokolowski-Tinten, Th. Tschentscher, D. von der Linde and J. B. Hastings

*Science* **315** (5812), 633-636.
DOI: 10.1126/science.1135009